JCI insight

Protein kinase G1 regulates bone regeneration and rescues diabetic fracture healing

Nadine Schall,[1,2] Julian J. Garcia,[1,3] Hema Kalyanaraman,[1] Shyamsundar Pal China,[1] Jenna J. Lee,[3] Robert L. Sah,[3] Alexander Pfeifer,[2] and Renate B. Pilz[1]

[1]Department of Medicine, University of California, San Diego, La Jolla, California, USA. [2]Institute for Pharmacology and Toxicology, University of Bonn, Bonn, Germany. [3]Department of Bioengineering, University of California, San Diego, La Jolla, California, USA.

Bone fractures are a major cause of morbidity and mortality, particularly in patients with diabetes, who have a high incidence of fractures and exhibit poor fracture healing. Coordinated expression of osteoblast-derived vascular endothelial growth factor (VEGF) and bone morphogenic proteins (BMPs) is essential for fracture repair. The NO/cGMP/protein kinase G (PKG) signaling pathway mediates osteoblast responses to estrogens and mechanical stimulation, but the pathway's role in bone regeneration is unknown. Here, we used a mouse cortical-defect model to simulate bone fractures and studied osteoblast-specific PKG1-knockout and diabetic mice. The knockout mice had normal bone microarchitecture but after injury exhibited poor bone regeneration, with decreased osteoblasts, collagen deposition, and microvessels in the bone defect area. Primary osteoblasts and tibiae from the knockout mice expressed low amounts of *Vegfa* and *Bmp2/4* mRNAs, and PKG1 was required for cGMP-stimulated expression of these genes. Diabetic mice also demonstrated low *Vegfa* and *Bmp2/4* expression in bone and impaired bone regeneration after injury; notably, the cGMP-elevating agent cinaciguat restored *Vegfa* and *BMP2/4* expression and full bone healing. We conclude that PKG1 is a key orchestrator of VEGF and BMP signaling during bone regeneration and propose pharmacological PKG activation as a novel therapeutic approach to enhance fracture healing.

Introduction

More than 15 million people sustain bone fractures each year in the United States, and about 10% of these fractures are complicated by delayed healing or nonunion between the bone fragments (1). Patients with type 1 or type 2 diabetes have an increased risk of fractures, and diabetic patients frequently experience impaired fracture healing, sometimes leading to disastrous consequences, including loss of a limb (2). Fracture repair is regulated by cytokines, growth factors, and angiogenic factors. All 3 types of signaling molecules are required for recruitment of mesenchymal progenitor cells, their differentiation into osteoblasts and chondroblasts, and the coupling of angiogenesis and osteogenesis in regenerating bone (3, 4). Initially, a hematoma forms at the fracture site and induces influx of neutrophils and macrophages; later, with new blood vessel growth, mesenchymal osteochondral progenitors migrate to the site of injury (1). Fracture repair recapitulates some of the processes that occur during bone development: the mesenchymal progenitor cells proliferate and either differentiate directly into osteoblasts that lay down bone matrix, termed primary ossification, or form chondrocytes to produce a cartilaginous template that calcifies and is subsequently replaced by bone, termed secondary ossification (1). Fracture healing typically involves a combination of both processes, with primary ossification predominating in an immobilized, stable fracture and secondary ossification being enhanced by motion (1, 4). Cells of osteoblast lineage produce bone morphogenic protein 2 (BMP-2) and vascular endothelial growth factor (VEGF), which are both essential for all phases of fracture healing, as demonstrated in mice with (pre-)osteoblast-specific knockout of *Bmp2* or *Vegfa* (5, 6).

We and others have shown that NO is important for skeletal homeostasis and repair (7–9). Treating rats systemically with a general inhibitor of NO synthase (NOS) interferes with fracture healing, which is reversed with local administration of an NO donor (8). NO is normally generated by 3 NOS isoforms

expressed in regenerating bone, with NOS-2 induced early and NOS-1 and -3 expression increasing during later phases of fracture repair (8). Mice deficient in NOS-2 or -3 have osteoblast defects and exhibit non-union in a model of delayed fracture healing (9–11). NO is generated by osteoblasts and osteocytes in response to bone-active hormones, including estrogens, insulin, and thyroid hormone, and it is required for pro-proliferative and pro-survival effects of these hormones in osteoblastic cells (7, 12–14). NO is also necessary for the anabolic effects of mechanical loading in bone (7, 15). However, the mechanism(s) whereby NO influences fracture healing are unknown.

NO can regulate biological processes in 2 ways: directly through its function as a radical or indirectly via the second messenger cGMP. Many direct NO effects are mediated by S-nitrosyl modification of proteins, whereas cGMP-dependent NO effects require activation of soluble guanylyl cyclase (16). cGMP targets cyclic nucleotide-dependent ion channels, phosphodiesterases, and 2 PKG isoforms (gene names *Prkg1* and *Prkg2*) expressed in cells of chondroblast, osteoblast, and osteoclast lineage (7). cGMP-elevating agents stimulate osteoblast proliferation, differentiation, and survival and improve bone microarchitecture in estrogen- and insulin deficiency–induced osteoporosis (17, 18). The focus of studying cGMP effects in bone has been mainly on PKG2 because PKG2-deficient mice are dwarfs due to impaired chondroblast differentiation (19). The bone phenotype of mice with global PKG1 deficiency is unknown because these mice have a high perinatal mortality, and surviving mice suffer from malnutrition due to severe gastrointestinal dysfunction (20).

To examine the role of PKG1 in bone regeneration, we generated osteoblast-specific *Prkg1*-knockout mice (*Prkg1* OB-KO). We found that these mice had normal bone microarchitecture under basal conditions but exhibited reduced osteoblastic VEGF and BMP2/4 expression and profound impairment in bone regeneration after skeletal injury. Because we previously observed reduced NO signaling in osteoblasts from mice with streptozotocin-induced type 1 diabetes (18), we used diabetic mice to test the hypothesis that reduced PKG signaling impairs bone regeneration after injury and that PKG activation may improve fracture repair.

Results

Generation of mice with osteoblast-specific Prkg1 deletion. We crossed mice carrying *Prkg1* alleles flanked by *loxP* sites (*Prkg1*^fl/fl^) with mice expressing Cre recombinase under control of the 2.3-kb collagen1a1 promoter (Col1a1-CRE^Tg/+^) — both in a C57BL/6 background — to generate mice with osteoblast-specific *Prkg1* knockout (genotype Col1a1-CRE^Tg/+^ *Prkg1*^fl/fl^), as described in Supplemental Figure 1, A and B; supplemental material available online with this article; https://doi.org/10.1172/jci.insight.135355DS1. We and others have shown that the 2.3-kb Col1a1 promoter is specifically expressed in cells of osteoblastic lineage, from committed osteoblast precursors to mature osteocytes (21, 22). *Prkg1* mRNA in tibial bone shafts was reduced by more than 80% in transgene-positive *Prkg1* OB-KO mice compared with control, transgene-negative *Prkg1*^fl/fl^ littermates, while *Prkg2* mRNA was not significantly reduced (Figure 1A). *Prkg1* mRNA in the kidney, lung, and brain was similar in wild-type and KO mice (Supplemental Figure 1C). Immunohistochemical staining with a PKG1-specific antibody showed strong staining for PKG1 in osteoblasts lining the endosteal bone surfaces, whereas the same cells failed to stain in *Prkg1* OB-KO mice and appeared smaller and flatter (Figure 1B). However, megakaryocytes stained strongly for PKG1 in the bone marrow of *Prkg1* OB-KO mice, serving as a positive control (Figure 1B, "M").

Prkg1 OB-KO mice show reduced bone formation and osteoblastic gene expression. To determine whether PKG1 deficiency affected osteoblast functions, we measured expression of several osteoblast-specific genes in tibial bone. Alkaline phosphatase (*Alpl*), osteocalcin (*Bglap*), and collagen-1α1 (*Col1a1*) mRNAs were significantly reduced in tibiae of *Prkg1* OB-KO mice compared with control (Cre-negative) *Prkg1*^fl/fl^ littermates, whereas mRNA of the housekeeping gene hypoxanthine phosphoribosyltransferase (*Hprt*) was not different (Figure 1C).

Nevertheless, the number of osteoblasts on trabecular surfaces in mice of both genotypes were similar (Figure 1D). To measure osteoblast activity in vivo, we injected mice with the calcium-binding fluorochrome calcein at 7 and 2 days before euthanasia. Calcein labeling of newly formed bone (23) demonstrated reduced mineralizing surfaces, mineral apposition rates, and bone formation rates in *Prkg1* OB-KO mice, suggesting decreased osteoblast activity in these mice (Figure 1, E and F, for trabecular surfaces and Supplemental Figure 1D for endocortical surfaces). mRNA expression of the osteoclast regulator RANKL (*Tnfsf11*), produced largely by osteoblastic cells, and of osteoclast-specific cathepsin K (*Ctsk*) and tartrate-resistant acid phosphatase (*Acp5*) were the same in *Prkg1* OB-KO and control mice (Figure 1, G and H). Expression of the RANKL antagonist osteoprotegerin (*Tnfrsf11b*) was slightly higher in *Prkg1* OB-KO mice, but the mice had a normal number of osteoclasts on trabecular bone surfaces (Figure 1, G and I).
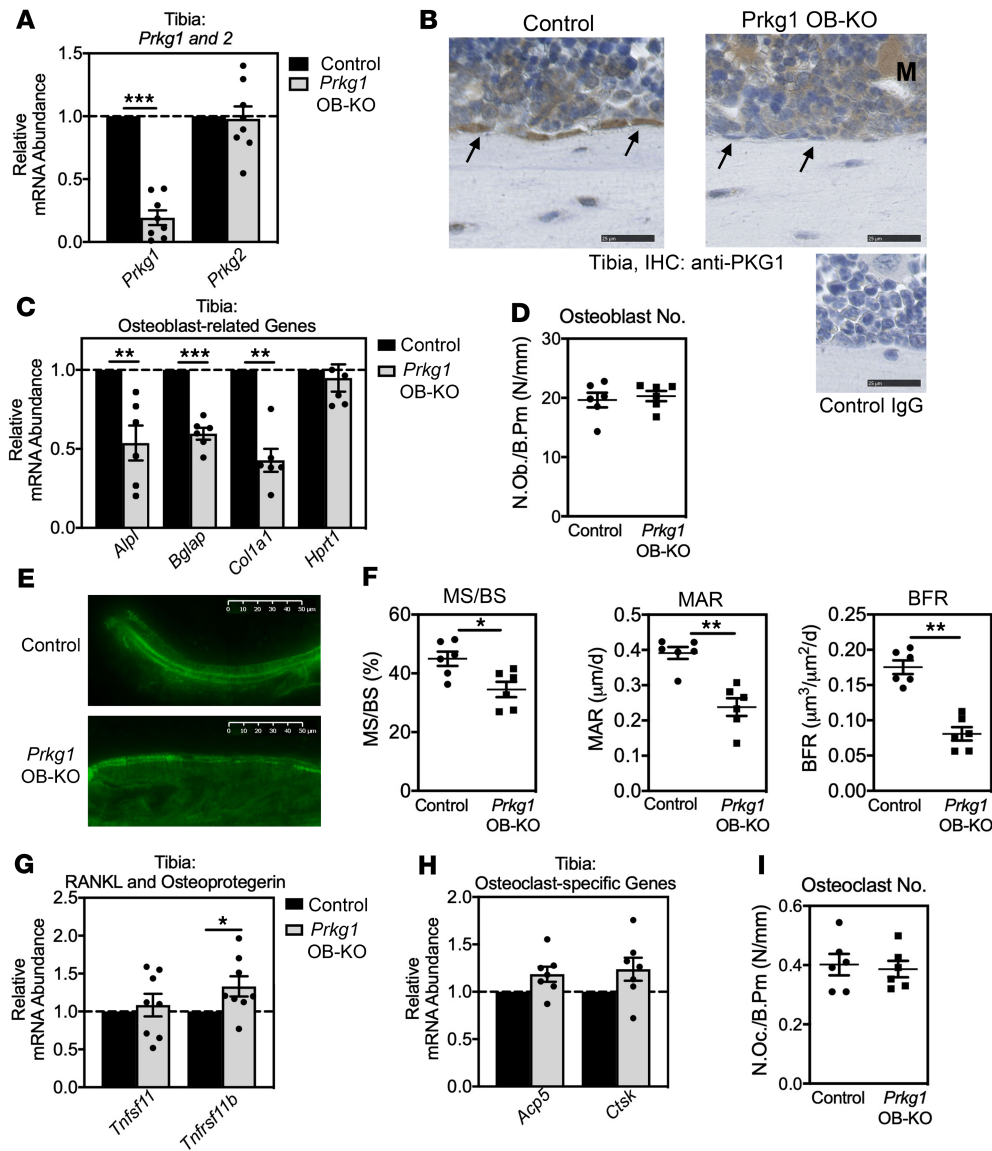
Figure 1. Reduced osteoblastic gene expression and bone formation rates in mice with osteoblast-specific *Prkg1* deletion. (**A**) *Prkg1* and *Prkg2* mRNA were quantified by quantitative reverse-transcription PCR (qRT-PCR) in control (genotype *Prkg1*fl/fl) and osteoblast-specific *Prkg1*-KO mice (*Prkg1* OB-KO, genotype Col1a1CRETg/+ *Prkg1*fl/fl); mRNA expression was normalized to 18S rRNA, and the mean relative mRNA level found in control mice was assigned a value of 1 (*n* = 7–8 mice per genotype). (**B**) Immunohistochemical staining with an antibody specific for PKG1 in tibial sections from control and *Prkg1* OB-KO mice (arrows point to osteoblasts; representative for 3 mice per genotype). Staining of megakaryocytes (M) served as positive control and control IgG as negative control (scale bars: 25 μm). (**C**) Expression of osteoblast differentiation-related genes (alkaline phosphatase, *Alpl*; osteocalcin, *Bglap;* collagen-1α1, *Col1a1*) and the housekeeping gene hypoxanthine phosphoribosyltransferase (*Hprt*) was measured in tibial bone of control (black bars) and *Prkg1* OB-KO mice (gray bars) and was normalized as described in panel **A** (*n* = 6 mice per genotype). (**D**) Osteoblasts were counted on trabecular surfaces of trichrome-stained tibial sections; values are expressed as number per millimeter of bone perimeter (*n* = 6 mice per genotype). (**E** and **F**) Control and *Prkg1* OB-KO mice, 8 weeks old, were injected with calcein at 7 and 2 days before euthanasia, respectively, and trabecular labeling was assessed by fluorescence microscopy of tibial sections. Mineralizing surfaces (MS/BS), mineral apposition rates (MARs), and bone formation rates (BFRs) were measured on trabecular surfaces as described in Methods (*n* = 6 mice per genotype). (**G** and **H**) Expression of RANKL (*Tnfsn11*) and osteoprotegerin (*Tnfrsf11b*) and of the osteoclast-specific genes tartrate-resistant acid phosphatase (TRAP; *Acp5*) and cathepsin K (*Ctsk*) was measured by qRT-PCR in control (black bars) and *Prkg1* OB-KO mice (gray bars) and normalized as described in panel **A** (*n* = 7–8 mice per genotype). (**I**) Osteoclasts were counted on trabecular surfaces of trichrome-stained tibial sections (*n* = 6 mice per genotype). Graphs show means ± SEM; *$P < 0.05$, **$P < 0.01$, and ***$P < 0.001$ by 1-sample *t* test (panels **A**, **C**, **G**) or 2-sided *t* test (**F**).

Prkg1 OB-KO mice have normal bone microarchitecture. *Prkg1* OB-KO mice and their control littermates had the same body weights and tibial lengths (Supplemental Figure 2A). In the absence of injury, 8-week-old male and female *Prkg1* OB-KO mice exhibited normal bone microarchitecture: μCT analysis of trabecular bone in the proximal tibia showed no differences in bone volume fraction, trabecular number, or bone mineral density between *Prkg1* OB-KO mice and control *Prkg1*fl/fl littermates (Supplemental Figure 2B shows

results for male mice, with similar results obtained in females). Cortical parameters, including cortical bone area fraction, cross-sectional thickness, and tissue mineral density measured at the midtibial diaphysis, were also the same in both genotypes (Supplemental Figure 2C for male mice, with similar results in females). Thus, osteoblast-specific PKG1 deletion had no effect on tibial bone microarchitecture in young, healthy mice, despite moderately decreased osteoblast activity in vivo (Figure 1, E and F), indicating that PKG1 is not required for basal skeletal homeostasis at that age, in the absence of fracture or bone damage.

Prkg1 is required for bone regeneration in a stable fracture model. Because *Prkg1* OB-KO mice showed reduced bone formation rates, we examined the effect of osteoblast-specific PKG1 ablation on bone regeneration in a fracture model. To study fracture healing equivalent to a stabilized fracture with primary ossification, we used a monocortical defect model, consisting of a 0.8-mm hole drilled through the anterior cortex of the tibia. This model has lower surgical complication rates and more reproducible histomorphometric changes than traditional fracture models (6, 24). In addition, it minimizes animal discomfort and does not interfere with normal ambulation; therefore, mechanical loading of the injured limb should not be affected (6, 25). Ten days after drilling a hole into the tibial cortex of 3-month-old C57BL/6 mice, the defect is partly bridged by newly formed, mineralized bone generated via primary ossification, i.e., direct differentiation of mesenchymal stem cells into osteoblasts without intercurrent chondrogenesis (25).

To minimize the influence of estrogens on NO/cGMP production (12, 21), we studied male mice. We analyzed their bones ex vivo using 3D μCT scans 10 days after surgery (Supplemental Figure 3). We found less mineralized tissue in the bony defects of *Prkg1* OB-KO mice compared with control *Prkg1*^{fl/fl} littermates: trabecular bone volume fraction (BV/TV), bone mineral density (BMD), and trabecular number in the defect were decreased in the KO mice, while trabecular spacing was increased (Figure 2, A and B).

To analyze the regenerating bone histologically, we made sagittal slices through the bone defect starting anteriorly and moving posteriorly and defined a 0.1-mm^2 area centered within the defect as an "area of interest" for analysis (Figure 2C). We analyzed only sections with an intact defect region, i.e., with 2 cortical ends flanking an intact area of interest at a distance of 0.8 mm. Less collagen was deposited in the area of interest, and a smaller number of osteoblasts lined newly formed bone in the defect of *Prkg1* OB-KO mice compared with control littermates (Figure 2, D and E); however, the number of TRAP+ osteoclasts in regenerating bone was similar in both genotypes (Figure 2, F and G). Thus, *Prkg1* OB-KO mice showed impaired bone regeneration after drill hole injury, suggesting important functions of cGMP/PKG signaling during bone healing, e.g., after a fracture.
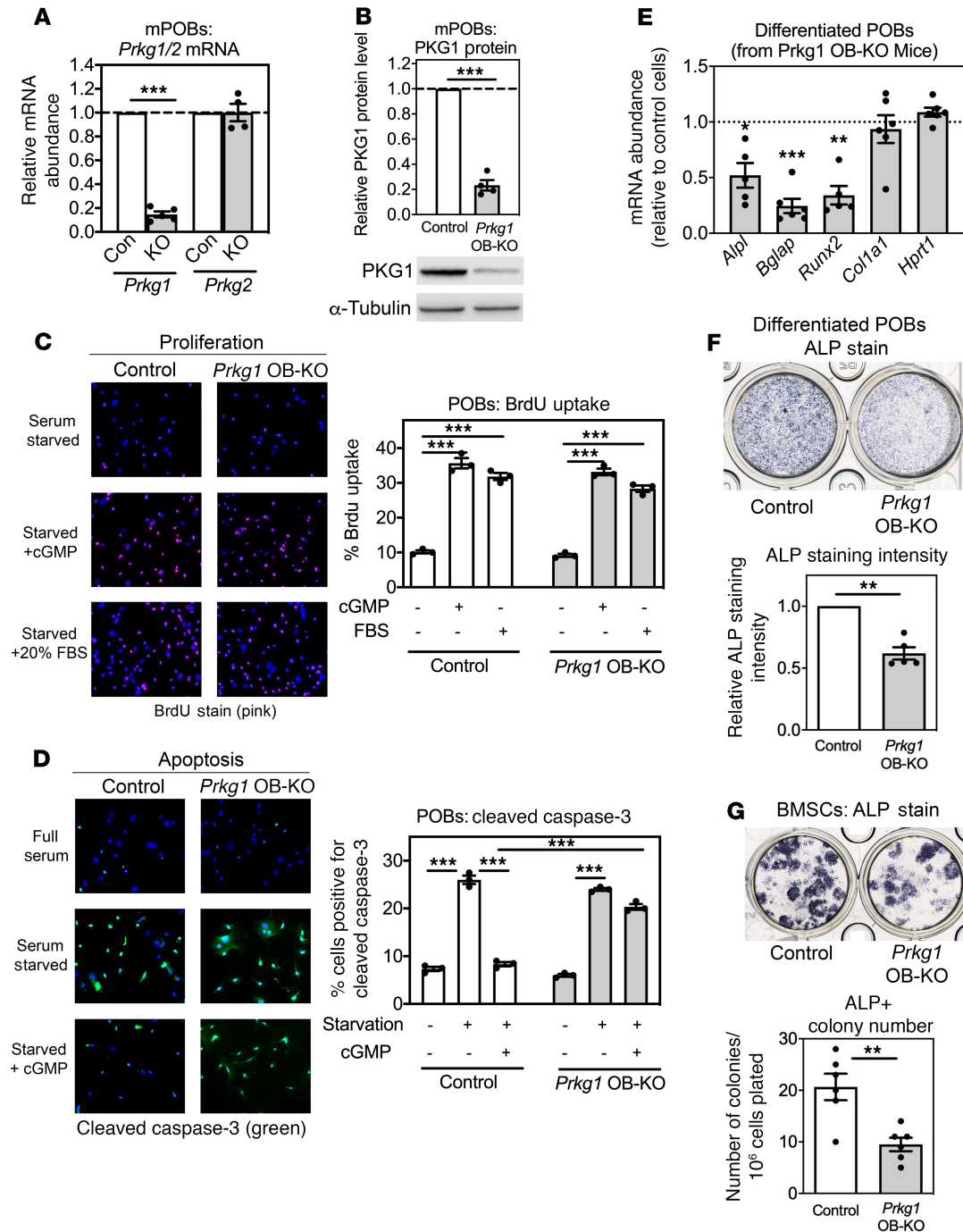
Prkg1-deficient osteoblasts proliferate normally but show impaired differentiation. To understand the cellular basis for *Prkg1* OB-KO mice exhibiting decreased bone regeneration after injury compared with their control *Prkg1*^{fl/fl} littermates, we isolated primary osteoblast(s) from long bones of both genotypes and examined their proliferation, survival, and differentiation potential. Primary osteoblasts (POBs) from *Prkg1* OB-KO mice showed more than 80% reduction in *Prkg1* mRNA expression compared with cells from control mice, with no difference in *Prkg2* mRNA expression (Figure 3A). The amount of PKG1 protein was decreased concomitantly (Figure 3B). PKG1-deficient and control osteoblasts proliferated similarly when stimulated with the membrane-permeable cGMP analog 8-CPT-cGMP or with 20% fetal bovine serum, measured after a period of growth factor deprivation in medium containing 0.1% FBS (Figure 3C). These data are consistent with PKG2, rather than PKG1, mediating proliferative responses of osteoblasts to various growth stimuli, including cGMP (18, 21, 26).

After incubation in serum-free medium, both PKG1-deficient and control POBs underwent apoptosis, as measured by cells staining positive for cleaved caspase-3 (Figure 3D). In control osteoblasts, 8-CPT-cGMP reduced apoptosis to values found in full growth medium, but cGMP was ineffective in *Prkg1* OB-KO osteoblasts (Figure 3D). These data suggest that PKG1-deficient osteoblasts may be less stress resistant under conditions of reduced growth factor supply and are consistent with NO/cGMP antiapoptotic effects being mediated by PKG (12).

After culture in differentiation medium, expression of the osteoblast differentiation-associated genes *Alpl* and *Bglap*, and of the osteoblastic transcription factor *Runx2*, was lower in osteoblasts from *Prkg1* OB-KO mice than in cells from control mice, while expression of *Col1a1* and *Hprt* mRNA was similar in the 2 cell types (Figure 3E). Alkaline phosphatase activity was reduced in differentiated PKG1-deficient POBs compared with control cells (Figure 3F). BMSCs isolated from *Prkg1* OB-KO mice formed less alkaline phosphatase–positive colonies in osteoblastic differentiation medium than BMSCs from control *Prkg1*^{fl/fl} mice, suggesting reduced differentiation capacity of PKG1-deficient osteoblast precursors (Figure 3G).
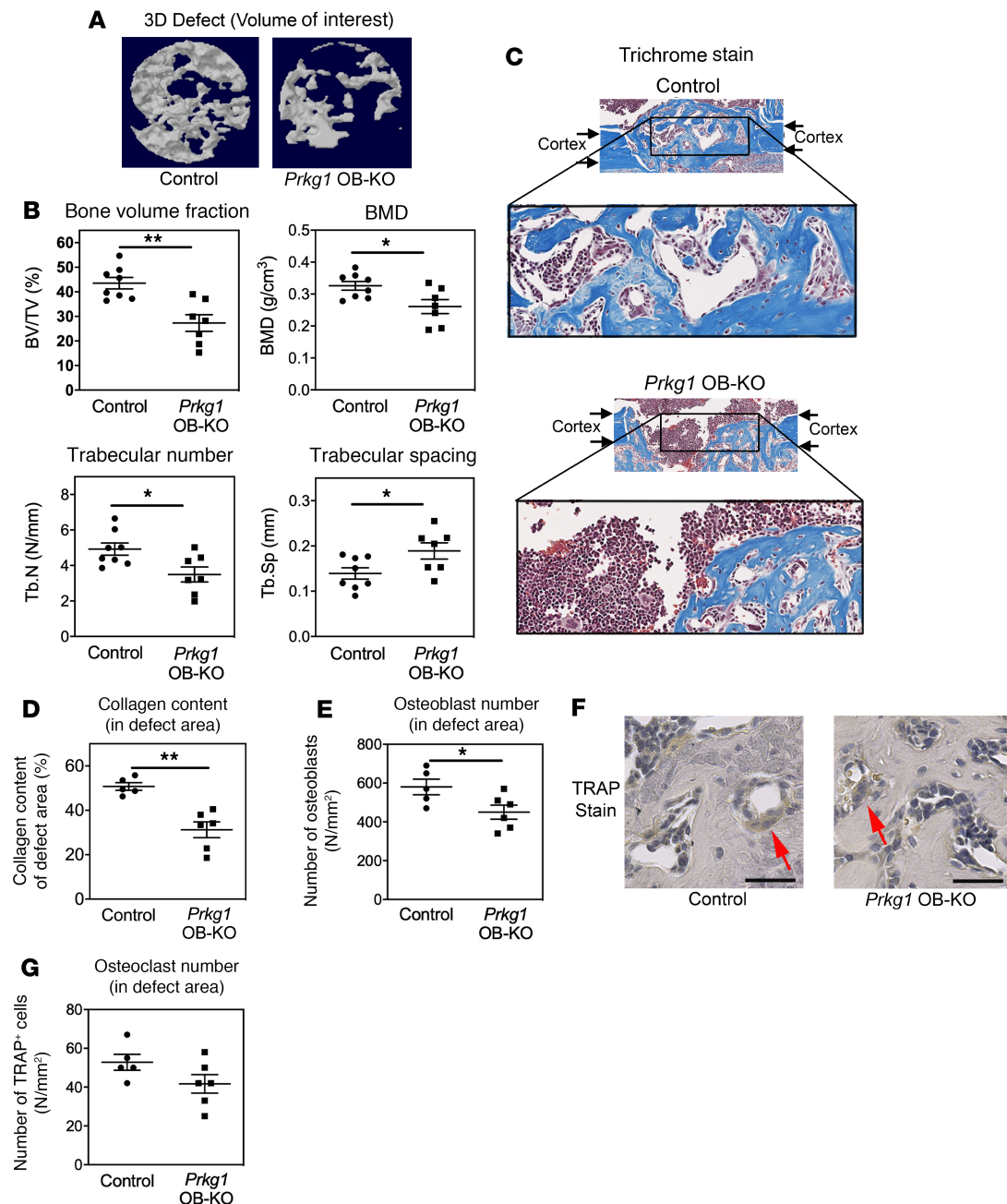
Figure 2. Impaired bone regeneration in *Prkg1* OB-KO mice. Male 10-week-old *Prkg1* OB-KO mice (Col1a1CRE[Tg/+] *Prkg1*^{fl/fl}) and control littermates (*Prkg1*^{fl/fl}) were placed under general anesthesia, and a 0.8-mm diameter burr hole was created on the anterior surface of the right tibia. Postoperative pain was controlled with buprenorphine for 3 days, and mice were euthanized 10 days after surgery. (**A**) μCT images of mineralized bone formed in the defect were reconstructed in 3D as described in Supplemental Figure 3. (**B**) 3D structural parameters of regenerating, mineralized bone in the defect were analyzed by μCT as described in Methods: bone volume fraction (BV/TV), bone mineral density (BMD), trabecular number (Tb.N), and trabecular spacing (Tb.Sp) were determined in the "volume of interest" (VOI), a cylinder with a diameter of 0.65 mm and a height of 0.3 mm centered in the cortical defect, as described in Supplemental Figure 3 ($n = 8$ control mice and $n = 7$ *Prkg1* OB-KO mice). (**C** and **D**) Collagen stained by aniline blue was measured using ImageJ (NIH) on trichrome-stained sections within a 0.1-mm^2 "region of interest" in the defect of the injured tibiae (enlarged; original magnification, ×40). This region of interest is marked by a black rectangle in panel **C** and was defined as an area 200 μm × 500 μm centered between the 2 cortical bone ends (marked by arrows). Collagen content was defined as percentage of blue-stained area within the area of interest. (**E**) Osteoblasts attached to newly formed bone surfaces (BSs) in the region of interest (defined in panel **C**) were counted on trichrome-stained sections. (**F** and **G**) Osteoclasts attached to newly formed bone were identified by TRAP staining; multinucleated TRAP+ cells were counted in the region of interest (scale bars: 40 μm). Data in **D**, **E**, and **G** represent means ± SEM for $n = 5$ control mice and $n = 6$ *Prkg1* OB-KO mice. *$P < 0.05$, and **$P < 0.01$ for the indicated pairwise comparisons by 2-sided *t* test (with similar results by Wilcoxon's rank-sum test).

Figure 3. Normal proliferation but altered apoptosis and gene expression of *Prkg1*-deficient osteoblasts. Primary osteoblasts (POBs, **A–F**) and bone marrow stromal cells (BMSCs, **G**) were isolated from long bones and bone marrow, respectively, of 8-week-old *Prkg1* OB-KO mice (Col1a1CRE[Tg/+] *Prkg1*^{fl/fl}) and control littermates (*Prkg1*^{fl/fl}). (**A**) *Prkg1* and *Prkg2* mRNAs were analyzed by qRT-PCR; mRNA concentrations were normalized to 18S rRNA, and the mean mRNA level in cells from control mice was assigned a value of 1 (n = 4 POB preparations per genotype). (**B**) PKG1 protein was assessed by Western blotting of whole-cell lysates using an anti-PKG1 antibody, with tubulin serving as a loading control and blots quantified by densitometry scanning (POBs from n = 4 mice per genotype). (**C**) POBs were cultured in medium with 0.5% FBS for 24 hours before receiving vehicle, 100 μM 8-CPT-cGMP, or 20% FBS for 1 hour, then 200 μM BrdU for 16 hours. BrdU incorporation into DNA of S-phase nuclei was detected by immunofluorescence (red; DNA counterstained with Hoechst 33342), with more than 200 cells analyzed per condition (means ± SEM of 3 independent experiments). (**D**) POBs were serum starved in medium containing 0.1% BSA for 24 hours or kept in normal growth medium with 10% FBS; some cells received 100 μM 8-CPT-cGMP. Apoptosis was measured as percentage of cells stained positive for cleaved caspase-3 (green); a minimum of 200 cells were analyzed per condition (means ± SEM of 3 independent experiments). (**E**) Confluent POBs were cultured for 14 days in differentiation medium, and mRNA transcripts were quantified by qRT-PCR (gene names as in Figure 1C); data were normalized as in panel **A** (POBs from n = 5–6 mice per genotype). (**F**) Confluent POBs or (**G**) BMSCs plated at 4×10^5 cells/cm² were cultured in osteoblastic differentiation medium for 14 days. POBs and BMSC colonies were stained for alkaline phosphatase (ALP) activity; (**F**) staining intensity was quantified by ImageJ, and (**G**) the number of ALP⁺ BMSC colonies was counted. Data represent means ± SEM for cells from n = 5–6 mice per genotype. **$P < 0.01$, and ***$P < 0.001$ for the comparison with control cells by 1-sample t test (panels **A**, **B**, **E**, and **F**) or 2-sided t test (**G**) or for the indicated comparisons by 2-way ANOVA (**C** and **D**).

Decreased osteoblastic Vegfa and Vegfr1 mRNA expression and reduced capillary density in regenerating bone of Prkg1 OB-KO mice. VEGF regulates angiogenesis and bone repair; it is essential for coupling osteogenesis with angiogenesis in regenerating bone and directly regulates osteoblast differentiation and function (6, 27). Osteoblasts are a major source of VEGF (*Vegfa*) in bone and express VEGF receptor-1 (*Vegfr1*) (27). NO/cGMP regulates VEGF production in smooth muscle (28), but it is not known whether crosstalk between these 2 signaling pathways exists in osteoblasts. We found that tibiae and primary osteoblasts isolated from *Prkg1* OB-KO mice expressed significantly less *Vegfa* and *Vegfr1* mRNA compared with bones and cells from control *Prkg1*$^{fl/fl}$ littermates (Figure 4, A and B; *Hprt* served as a control for RNA quality). Treating control osteoblasts with 8-CPT-cGMP for 24 hours increased both *Vegfa* and *Vegfr1* mRNA expression, whereas the drug had no effect in PKG1-deficient osteoblasts (Figure 4, C and D). Thus, in osteoblasts, *Vegfa* and *Vegfr1* expression is regulated by cGMP/PKG1, and PKG1 is required for basal expression of both growth factor and receptor.

To examine the effects of decreased osteoblastic *Vegfa* expression in *Prkg1* OB-KO mice, we examined capillary density in regenerating bone by staining endothelial cells and endothelial cell clusters with antibodies specific for CD31 (platelet/endothelial cell adhesion molecule-1). We found significantly less staining, indicating reduced capillary density, in regenerating bone of *Prkg1* OB-KO mice compared with control littermates (Figure 4E). These data show that cGMP/PKG1 signaling is required for the angiogenic response during bone repair.

Impaired BMP2/4 expression and Smad signaling in POBs and bones from Prkg1 OB-KO mice. BMP signaling is crucial for all stages of bone repair (5, 29). BMP-2 and -4 stimulate osteoblast differentiation and enhance angiogenesis by stimulating osteoblast-derived *Vegfa* expression (5, 29, 30). Therefore, we sought to examine *Bmp2/4* and *Bmpr1/2* expression. Because PKG1 modulates BMP signaling in C212 myoblasts via association with the BMP receptor-2 (31), we also assessed BMP-stimulated Smad1/5/8 phosphorylation in bones and osteoblasts of *Prkg1* OB-KO mice.

We found that transcripts encoding BMP-2/4 and BMP receptor-2 were significantly lower in tibiae and primary osteoblasts from *Prkg1* OB-KO mice compared with control littermates, whereas *Bmpr1a* mRNA was unaltered (Figure 5, A and B). Immunohistochemical staining for BMP2/4 was reduced in endocortical osteoblasts on bone sections from *Prkg1* OB-KO mice compared with sections from control mice, supporting reduced BMP production by PKG1-deficient cells of osteoblastic lineage (Supplemental Figure 4A). 8-CPT-cGMP increased *Bmp2/4* and *Bmpr2* mRNA expression in control osteoblasts but not in *Prkg1* OB-KO osteoblasts; *Bmpr1a* mRNA was unaffected by cGMP (Figure 5C). BMP2-induced Smad 1/5/8 phosphorylation was significantly reduced in *Prkg1* OB-KO osteoblasts (Figure 5D), indicating impaired BMP signaling downstream of the BMP receptor, similar to results in C2C12 cells (31). Consistent with these findings, BMP-induced *Alpl* mRNA expression was less in *Prkg1* OB-KO osteoblasts compared with control cells (Supplemental Figure 4B). Thus, PKG1 regulates *Bmp2/4* and *Bmpr2* expression and Smad signaling downstream of the BMP receptor in osteoblasts.

To examine the effects of decreased *Bmp2/4* and *Bmpr2* expression in osteoblasts of *Prkg1* OB-KO mice in vivo, we examined Smad phosphorylation in endocortical osteoblasts under basal conditions and after injury in regenerating bone by immunohistochemical staining with antibodies specific for active Smad1/5/8 phosphorylated on Ser463/465. Phospho-Smad1/5/8 staining of osteoblasts lining the tibial surfaces of uninjured *Prkg1* OB-KO mice was reduced compared with the strong staining in osteoblasts of control mice (Supplemental Figure 4C). In *Prkg1* OB-KO mice subjected to a cortical drill hole, the number of nuclei staining positive for phospho-Smad1/5/8 was reduced in regenerating bone (in the region of interest between the 2 cortical ends), compared with the same region in *Prkg1*$^{fl/fl}$ control mice (Figure 5E). These results are consistent with decreased Smad signaling in PKG1-deficient osteoblasts.

PKG activation rescues bone regeneration in mice with type 1 diabetes. Fracture healing in patients with diabetes is frequently delayed and has a high risk of complications, including nonunion (2). Endothelial NO generation and systemic cGMP concentrations are reduced in patients with diabetes and mice with type 1 diabetes (18, 32). We previously showed that NO/cGMP signaling is impaired in osteoblasts exposed to high glucose, but PKG can be efficiently activated using cinaciguat, an NO-independent activator of soluble guanylyl cyclase (18). We hypothesized that cinaciguat might improve bone healing in mice with type 1 diabetes.

To induce diabetes, we administered streptozotocin to 10-week-old male C57BL/6 mice, using male mice again to minimize estrogen effects on NO/cGMP production (12, 21). Drill hole surgery was performed 4 weeks later (after mice had been hyperglycemic for at least 2 weeks), and on postoperative day 1, we started daily cinaciguat injections until euthanasia on day 10 (Figure 6A). We previously showed that this dose of
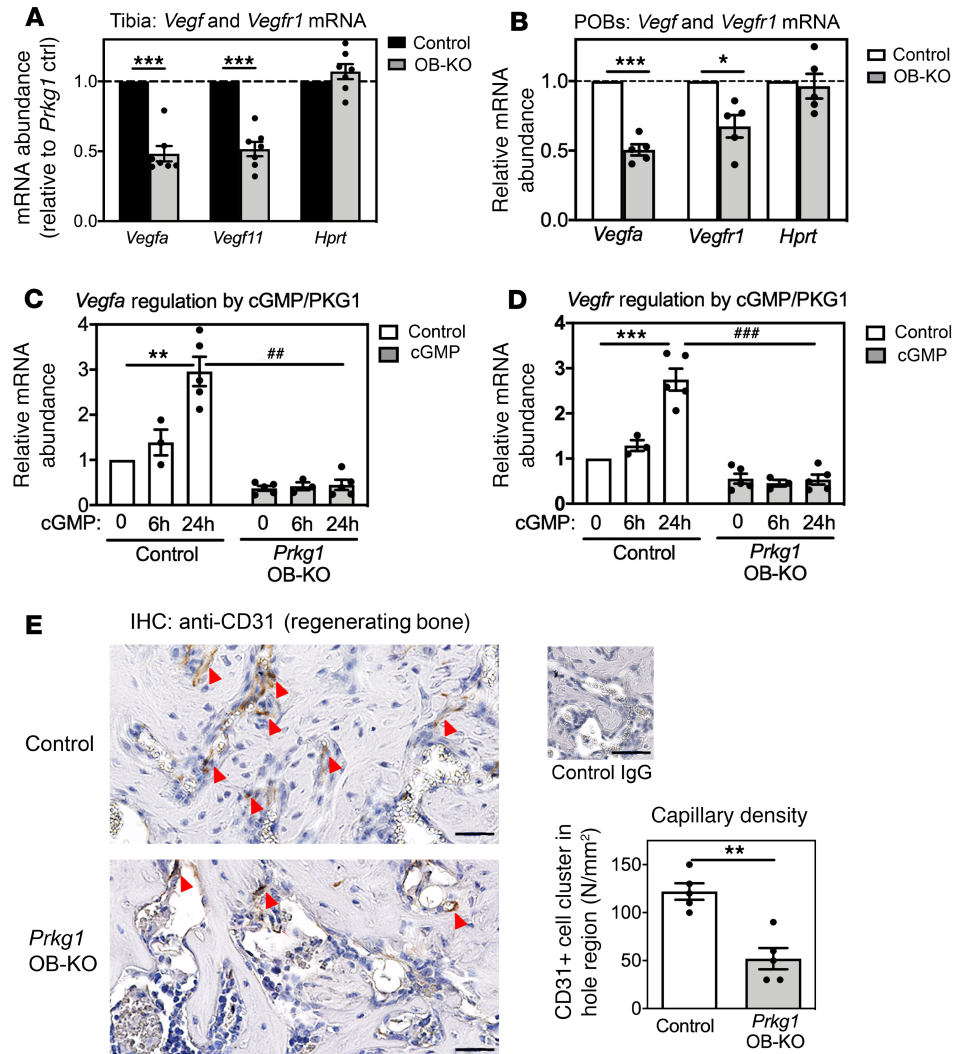
Figure 4. Reduced *Vegfa* and *Vegfr1* expression in PKG1-deficient osteoblasts and bones and decreased capillary density in regenerating bone of *Prkg1* OB-KO mice. (**A**) Transcripts of vascular endothelial growth factor A (*Vegfa*), and its receptor (*Vegfr1*), were quantified by qRT-PCR together with *Hprt* mRNA in tibiae of *Prkg1* OB-KO mice (Col1a1CRE$^{Tg/+}$ *Prkg1*$^{fl/fl}$) and control littermates (*Prkg1*$^{fl/fl}$); mRNA amounts were normalized to 18S rRNA, and the mean mRNA level found in control tibiae was assigned a value of 1 (n = 7 mice per genotype). (**B**) *Vegfa*, *Vegfr1*, and *Hprt* mRNAs were measured in POBs isolated from *Prkg1* OB-KO and control mice. Values were normalized to 18S rRNA, and the mean mRNA level found in control cells was assigned a value of 1 (n = 5 independent experiments). (**C** and **D**) POBs from control and *Prkg1* OB-KO mice were cultured in medium containing 0.5% FBS for 24 hours before receiving 100 μM 8-CPT-cGMP (gray bars) for 6 or 24 hours, as indicated. (**C**) *Vegfa* and (**D**) *Vegfr1* mRNAs were quantified and normalized to the mean level of vehicle-treated control cells as described in panel **B** (n = 3 independent experiments for 6 hours and n = 5 for 0- and 24-hour time points). (**E**) *Prkg1* OB-KO mice and control littermates were subjected to drill hole surgery as described in Figure 2. Immunostaining was performed with anti-CD31 antibody (or control IgG) on longitudinal tibial sections through the drill-generated defect; shown is the 0.1-mm² "region of interest," defined as in Figure 2C. Capillary density was assessed based on single CD31-immunoreactive endothelial cells and endothelial cell clusters separate from other microvessels (red arrowheads); the graph represents n = 5 mice/genotype. Graphs show means ± SEM; *$P < 0.05$, **$P < 0.01$, and ***$P < 0.001$ for comparison by 1-sample t test (**A** and **B**), 2-sided t test (**E**), or 2-way ANOVA (**C** and **D**); ##$P < 0.01$, and ###$P < 0.001$ for the comparison with control cells under the same treatment condition.

cinaciguat increases serum cGMP concentrations in control and diabetic animals and restores cGMP in diabetic mice to levels found in control mice without affecting systolic blood pressure (18). The diabetic mice lost on average 15% of their body weight compared with nondiabetic controls, and cinaciguat treatment had no effect on the weight of control or diabetic mice (Supplemental Figure 5A). Similarly, cinaciguat did not affect the blood glucose concentrations in control or diabetic mice (Supplemental Table 1). Diabetic mice showed
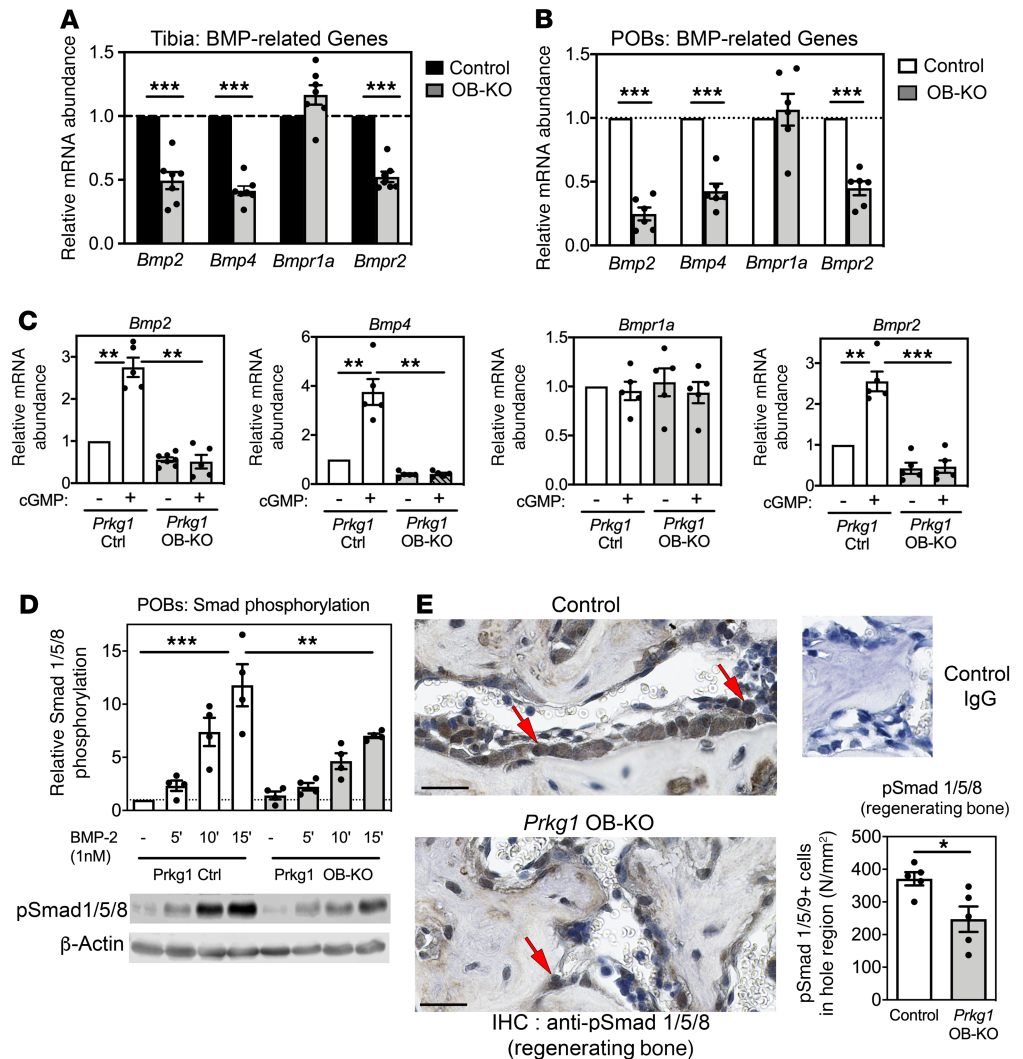
Figure 5. Impaired BMP2/4 expression and BMP signaling in POBs and bones from *Prkg1* OB-KO mice. (**A**) Transcripts of BMPs (*Bmp2* and *Bmp4*) and their receptors (*Bmpr1a* and *Bmpr2*) were quantified by qRT-PCR in tibiae of *Prkg1* OB-KO mice (Col1a1CRE[Tg/+] *Prkg1*^{fl/fl}) and control littermates (*Prkg1*^{fl/fl}); mRNA levels were normalized as in Figure 4A (*n* = 7 mice per genotype). (**B**) BMP-related transcripts were measured in POBs isolated from *Prkg1* OB-KO and control mice. Values were normalized as described in Figure 4B (*n* = 6 independent experiments). (**C**) POBs from control and *Prkg1* OB-KO mice were cultured in medium containing 0.5% FBS for 24 hours before receiving 100 μM 8-CPT-cGMP (gray bars) for 24 hours. *Bmp2*, *Bmp4*, *Bmpr1*, and *Bmpr2* mRNAs were quantified and normalized as in Figure 4B, with levels in vehicle-treated control cells assigned a value of 1 (*n* = 3 independent experiments for 6 hours and *n* = 5 for 0- and 24-hour time points). (**D**) POBs from control and *Prkg1* OB-KO mice were cultured as in panel **C** but received vehicle or 1 nM BMP-2 for the indicated times, and Smad-1/5/8 phosphorylation was assessed by Western blotting using Smad-pSer463/465–specific antibodies. Blots were quantified by ImageJ and normalized to β-actin (*n* = 4 independent experiments). (**E**) *Prkg1* OB-KO mice and control littermates were subjected to drill hole surgery as described in Figure 2. Immunostaining was performed with phospho-Smad1/5/8 (pSer463/465) antibody (or control IgG) on longitudinal tibial sections through the drill-generated defect. Phospho-Smad1/5/8–positive brown nuclei (red arrows show examples, scale bars: 25 μm) were counted in the 0.1-mm² "region of interest" (defined in Figure 2C). The graph summarizes results for *n* = 5 *Prkg1* mice per genotype. Graphs show means ± SEM; *$P < 0.05$, **$P < 0.01$, and ***$P < 0.001$ for comparison by 1-sample *t* test (**A** and **B**), 2-sided *t* test (**F**), or 2-way ANOVA (**C** and **D**).

severely reduced bone regeneration compared with control mice, with lower BV/TV, BMD, and trabecular number and increased trabecular spacing in the defect (Figure 6, B and C). However, cinaciguat restored all 4 parameters in the diabetic mice to levels found in control animals; in control mice, cinaciguat similarly increased BV/TV, with a trend toward increased BMD and trabecular number in regenerating bone (Figure 6, B and C). Diabetic mice had less collagen deposition and a lower number of osteoblasts in the bony defects compared with control animals, but cinaciguat restored collagen deposition and increased osteoblast numbers
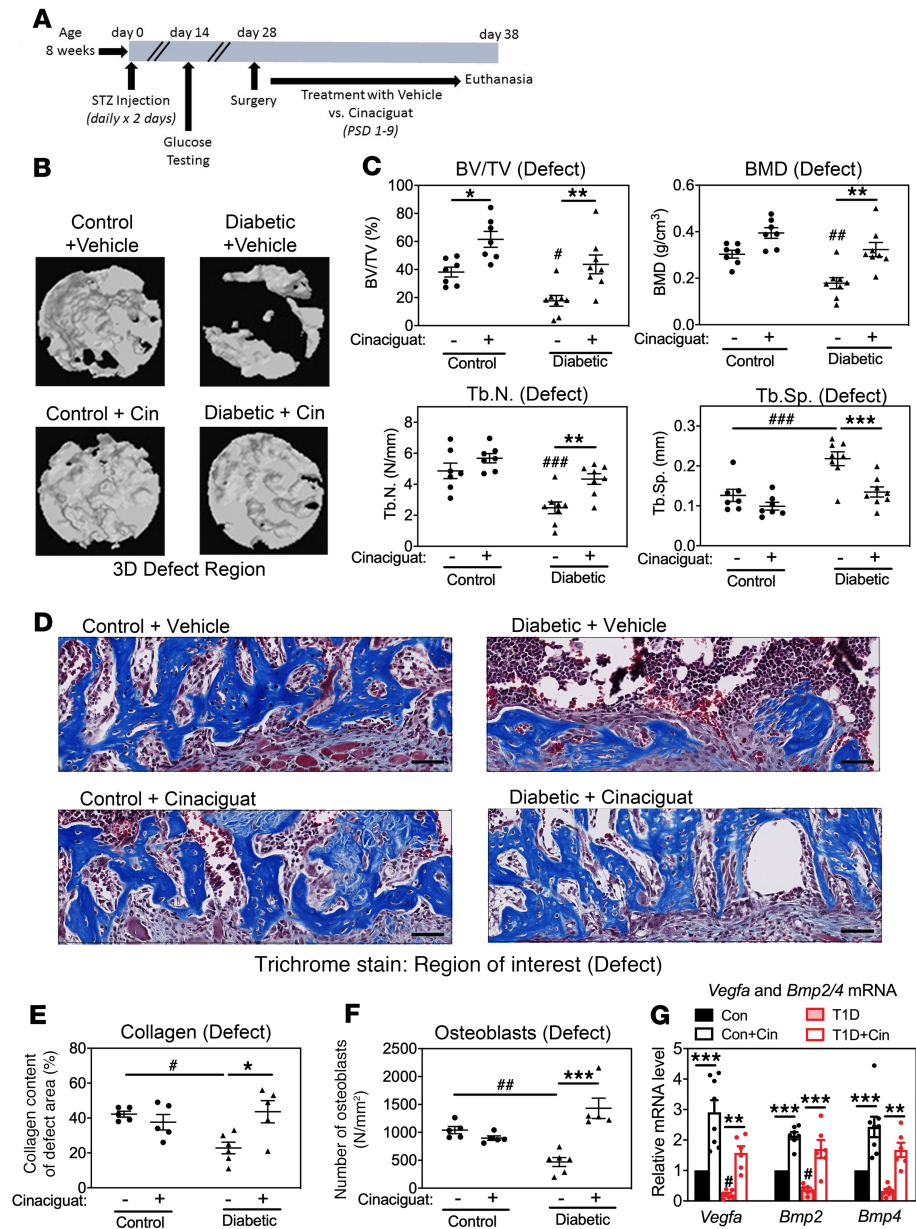
Figure 6. PKG activation rescues bone regeneration in mice with type 1 diabetes. (**A**) Male mice, 10 weeks old, received vehicle (Control) or 2 doses of streptozotocin (STZ) to induce type 1 diabetes, and blood glucose was measured 14 days later. Twenty-eight days after the start of STZ, control and diabetic mice (glucose > 290 mg/dL) received a 0.8-mm burr hole on the anterior surface of the right tibia, as described in Figure 2. On postsurgical days (PSD) 1–9, mice were given daily intraperitoneal injections of either vehicle or cinaciguat (10 μg/kg/d), and they were euthanized on PSD 10. (**B**) μCT images of mineralized bone formed in the drill hole defect were reconstructed in 3D as described in Supplemental Figure 3. (**C**) Bone volume fraction (BV/TV), bone mineral density (BMD), trabecular number (Tb.N), and trabecular spacing (Tb.Sp) were determined in the "volume of interest," centered in the cortical defect, as described in Figure 2B (n = 7 mice in each of the control groups, and n = 8 mice in each of the diabetic groups). (**D** and **E**) Collagen stained by aniline blue was measured on trichrome-stained sections, as described in Figure 2C, in the 0.1-mm² "region of interest" in the defect of the injured tibiae (n = 5–6 mice per group; scale bars: 50 μm). (**F**) Osteoblasts attached to newly formed BSs in the region of interest were counted on trichrome-stained sections (n = 5–6 mice per group). (**G**) *Vegfa*, *Bmp2*, and *Bmp4* mRNAs were quantified by qRT-PCR in tibiae of control and diabetic mice treated with vehicle or cinaciguat (Cin); mRNA amounts were normalized to 18S rRNA, and the mean mRNA level found in tibiae of vehicle-treated control mice was assigned a value of 1 (n = 6–7 mice per group). The graphs show means ± SEM; *P < 0.05, **P < 0.01, and ***P < 0.001 for the indicated pairwise comparisons by 2-way ANOVA. #P < 0.05, ##P < 0.01, and ###P < 0.001 for the comparison with untreated control mice.
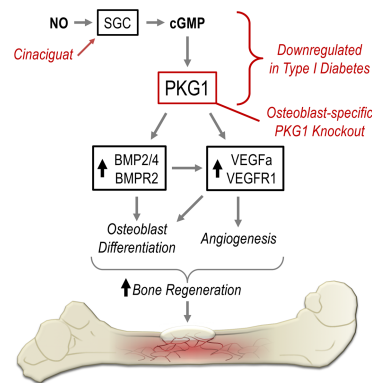
Figure 7. PKG1 regulation of bone regeneration via BMP and VEGF. Soluble guanylyl cyclase (SGC) generates cGMP in response to NO (or stimulation by cinaciguat) to activate PKG1, which in turn increases expression of *Bmp2/4*, *Vegfa*, and their receptors *Bmpr2* and *Vegfr1* in osteoblasts. BMP and VEGF are known to control osteoblast differentiation and angiogenesis and are crucial for all phases of fracture repair. Osteoblast-specific deletion of PKG1 or downregulation of NO/cGMP/PKG signaling in diabetic osteoblasts leads to impaired bone regeneration, but NO-independent SGC stimulation by cinaciguat in diabetic mice rescues fracture healing.

in the diabetic animals (Figure 6, D–F). Osteoclasts were not different in the regenerating bone of diabetic versus control mice, and cinaciguat did not affect osteoclast number (Supplemental Figure 5B). Cinaciguat also improved bone regeneration in healthy female mice (Supplemental Figure 5C).

Cinaciguat increased *Vegfa* and *Bmp2/4* mRNA expression in tibial shafts of control and diabetic mice (Figure 6G), consistent with its ability to increase serum cGMP concentrations and its capacity to restore cGMP/PKG signaling in mice with streptozotocin-induced diabetes (18). The tibiae of diabetic mice contained less *Vegfa*, *Bmp2/4*, and *Bmpr2* mRNAs compared with bones of control mice, but cinaciguat fully rescued expression of all 4 genes (Figure 6G and Supplemental Figure 5D). Expression of *Bmpr1a* and *Hprt* was not altered in diabetic bones and not affected by cinaciguat (Supplemental Figure 5D). The decrease in *Vegfa*, *Bmp2/4*, and *Bmpr2* mRNAs in the bones of diabetic compared with control mice is consistent with decreased NO/cGMP signaling in osteoblasts of mice with streptozotocin-induced type 1 diabetes (18) and in keeping with reduced expression of these genes in *Prkg1* OB-KO mice (Figures 4A and 5A). These data indicate a potentially novel and important role for PKG regulation of VEGF and BMP-2/4 during fracture healing.

Discussion

Mice with osteoblast-specific deletion of *Prkg1* showed decreased mineral apposition and bone formation rates and decreased expression of *Bmp2/4* and *Vegfa* and osteoblastic differentiation genes (e.g., osteocalcin). However, at 8 weeks of age, these KO mice had no decrease in basal trabecular or cortical bone volumes compared with their wild-type littermates, despite the decrease in osteoblast activity, which was not compensated for by a decrease in osteoclasts. Mice with osteoblast-specific deletion of the Wnt coreceptor *Lrp5* also have normal bone microarchitecture at the age of 8 weeks, despite severely reduced bone formation rates; however, they develop low trabecular and cortical bone volumes by 6 months of age (33). Our primary objective was to study bone repair, but it is possible that the *Prkg1* OB-KO mice may develop altered bone microarchitecture later in life.

The osteoblast deficiencies found in *Prkg1* OB-KO mice impaired bone healing after drill hole injury, which simulates a stable bone fracture. Bone healing after such an injury occurs predominantly via primary ossification with differentiation of mesenchymal progenitor cells into osteoblasts (6, 25). The periosteum is thought to be the major source of progenitor cells, but endosteum-derived progenitor cells and BMSCs contribute to bone healing (1, 34). These 3 stem cell populations may contribute differentially to bone regeneration versus bone growth and homeostasis, and PKG1 expression and/or functions may differ in these stem cell compartments, potentially explaining why bone repair was severely affected in *Prkg1* OB-KO mice while bone microarchitecture was not — at least in young mice; this requires further investigation.

Overall, our data show that PKG1 is a major regulator of angiogenic and osteogenic signaling pathways during bone repair. Our search for mechanism(s) whereby PKG1 regulated bone regeneration revealed a potentially previously unknown crosstalk between cGMP/PKG1 and the VEGF and BMP pathways (Figure 7). Bone regeneration requires the concerted action of both VEGF and BMP-2 signaling, with BMP-2

enhancing osteoblast-derived *Vegfa* expression (5, 6, 30). VEGF is a key mediator of angiogenesis and stimulates multicellular crosstalk during bone repair. It couples osteogenesis to angiogenesis and directly controls the differentiation and function of osteoblasts (6, 27). Pharmacological or genetic inhibition of VEGF signaling inhibits bone repair via both primary and secondary osteogenesis (6, 35, 36). The reduced *Vegfa* and *Vegfr1* expression found in bones and osteoblasts from *Prkg1* OB-KO mice correlated with decreased capillary density in regenerating bone and likely played a major role in decreased fracture healing. The NO/cGMP/PKG1 signaling pathway may function both upstream and downstream of VEGF: NO stimulates *Vegf* mRNA and protein expression in smooth muscle (28), and it mediates VEGF-induced endothelial cell proliferation, migration, and tube formation (37–39). cGMP-elevating agents enhance angiogenesis in response to hind limb ischemia, and ischemia-induced angiogenesis is severely impaired in soluble guanylyl cyclase– or PKG1-deficient mice (40, 41). The mechanism of cGMP/PKG1 stimulation of *Vegfa* and *Vegfr1* mRNA expression in osteoblasts may involve PKG1 activation of the cAMP-responsive element-binding protein (CREB) because CREB is required for both *Vegfa* and *Vegfr1* promoter activity, and PKG1 phosphorylates CREB, thereby activating CREB-dependent transcription (42–44).

BMP-2/4 and BMP receptor-2 expression is strongly induced during fracture repair, and mice lacking the ability to produce BMP in their limb bones completely fail to heal fractures (5, 45). Conditional global BMP2- and BMP4-KO mice display low-turnover bone loss and impaired bone regeneration (46). Recombinant BMPs are used to treat open fractures and fracture nonunions in humans, and clinical studies indicate that BMP2 treatment reduces the need for surgical revisions and bone grafting (47). BMP2/4 stimulate angiogenesis in bone explant cultures via increased osteoblastic VEGF production, and BMP2/4 act synergistically with VEGF to enhance bone regeneration (30, 48). To our knowledge, *Bmp2/4* and *Bmpr2* regulation by cGMP has not been previously observed. However, our observation of impaired Smad-1/5/8 signaling downstream of the BMP receptor, with decreased Smad phosphorylation in BMP-2–treated, PKG1-deficient osteoblasts and bones from *Prkg1* OB-KO mice, is consistent with previous reports of PKG1 enhancing Smad phosphorylation and transcription via interaction with BMP receptor-2 (31). Impaired bone regeneration in *Prkg1* OB-KO mice is at least in part attributable to decreased *Bmp2/4* and *Bmpr2* expression and BMP signaling, and we identified a potentially novel mechanism whereby BMP ligand and receptor expression in osteoblasts can be upregulated by pharmacological means, i.e., via cGMP-elevating agents, to improve fracture healing.

Patients with type 1 or type 2 diabetes have an increased risk of fractures, and these fractures can occur with minimal trauma because of bone loss with type 1 and altered bone material quality with type 1 and 2 diabetes (2). Patients with diabetes experience poor fracture healing, especially in the presence of microvascular complications and poor long-term glycemic control (2). In osteoblasts exposed to high glucose, NO/cGMP signaling is impaired due to O-Glc-*N*-acetylation of NO synthase-3 and oxidative inhibition of soluble guanylyl cyclase (18). Because poor wound healing in diabetes is associated with reduced VEGF expression (49), we hypothesized that impaired osteoblastic VEGF synthesis in diabetic bone may contribute to poor fracture healing and guanylate cyclase activation by cinaciguat may improve bone regeneration. In fact, we found low amounts of *Vegfa* and *Bmp2/4* mRNA in the bones of diabetic mice, and cinaciguat increased expression of these genes, consistent with cGMP/PKG1 regulation of *Vegfa* and *Bmp2/4* mRNA in osteoblasts. Cinaciguat restored bone regeneration in diabetic mice to levels found in control mice and also improved bone healing in nondiabetic mice, suggesting that pharmacological stimulation of VEGF and BMP synthesis may have broader applications in bone healing.

A limitation of our study is that we examined a model of stable fracture healing that proceeds largely via primary ossification. Whether PKG1 deficiency also affects callus formation and secondary ossification remains to be investigated. However, NO synthase inhibitors reduce callus formation and bone regeneration in an open fracture model, and this effect is reversed by local administration of an NO donor; the latter likely acts via cGMP (8). Mice with increased circulating C-type natriuretic peptide, which stimulates cGMP production via receptor guanylyl cyclase B, also show accelerated fracture healing in a traditional femur fracture model (50, 51). Both studies suggest that cGMP-elevating agents can enhance fracture healing via primary and secondary ossification, but the downstream effectors of cGMP were not examined so far.

Presently, there are no established pharmacological treatments to promote fracture healing, with the exception of local application of BMP at the time of surgery for nonunion fractures (47). Proper dosing of BMP has proved challenging, and trials with local application of VEGF have been disappointing, perhaps because of suboptimal dosing and delivery (6). Our results in *Prkg1* OB-KO mice suggest that the positive effects of cGMP on bone regeneration are mediated by PKG1 via regulation of VEGF and BMP signaling.

Several cGMP-elevating pharmacological agents are in clinical use, including NO-generating nitrates, phosphodiesterase-5 inhibitors, and soluble guanylyl cyclase stimulators. The major reason to use cinaciguat in this study was that this agent activates soluble guanylyl cyclase in an NO-independent manner, since oxidative stress present in diabetes and other conditions results in an NO-insensitive enzyme (18, 52). Taken together, cGMP-elevating agents could represent a novel treatment paradigm for patients with impaired fracture healing, especially where healing is compromised because of reduced angiogenesis, such as in elderly and diabetic patients (53).

Methods

Materials. Antibodies are listed in Supplemental Table 2. BrdU, deoxyribonuclease I (DNase I), anti-BrdU antibody, the Acid Phosphatase/Leucocyte (TRAP) Kit, and calcein were from MilliporeSigma. The cGMP analog 8-CPT-cGMP was from BioLog. Recombinant human BMP-2 was from HumanZyme.

Generation of osteoblast-specific Prkg1-KO mice. Mice carrying floxed *Prkg1* alleles (*Prkg1*fl/fl) were generated in a C57BL/6 background (54). Osteoblast-specific *Prkg1*-KO mice were obtained by crossing *Prkg1*fl/fl mice with transgenic mice expressing Cre recombinase under control of the 2.3-kb collagen type-1α1 promoter, B6.Cg-Tg(Col1a1-cre)-Haak mice (RIKEN BioResource Research Center Jackson Laboratory, also in a C57BL/6 background), as described in Supplemental Figure 1A. Mice were assessed for floxed *Prkg1* alleles and presence or absence of the Col1a1-Cre transgene by PCR, using DNA from tail biopsies (Supplemental Figure 1B). The floxed *Prkg1* allele was amplified using the following primers: 5′-GTGAAAATACTACTAGGTATCATGG-3′ and 5′-CATGTACTAAACATTAAGGGTAGAG-3′ to generate a 340-bp fragment, compared with a 244-bp fragment for the wild-type allele. The Cre transgene was detected with the following primers: 5′-CAAAACAG-GCTCTAGCGTTC-3′ and 5′-TCGACCAGTTTAGTTACCCC-3′. All mice were housed at 3–4 animals per cage in a temperature-controlled environment with a 12-hour light/12-hour dark cycle and ad libitum access to water and food (Teklad Rodent Diet 8604). Mice injured due to fighting were excluded from analysis.

Tibial monocortical defect model. Male 10-week-old mice were placed under general anesthesia by intraperitoneal injection of 100 mg/kg ketamine and 10 mg/kg xylazine. The lateral aspect of the right tibia was exposed, preserving the periosteum. An osseous hole (0.8 mm in diameter) was created through the anterior cortex of the tibia using a round burr attached to a dental drill (5000 rpm), with saline irrigation to remove bone fragments, as described previously (6). The soft tissue wound was closed by separately suturing the muscle and skin layers with 4-0 absorbable gut suture. After surgery, mice received a subcutaneous injection of 0.1 mg/kg buprenorphine-SR (release over 72 hours) for analgesia. Mice were monitored daily; all mice were ambulating normally after awakening from anesthesia. Ten days after surgery, mice were euthanized by CO_2 intoxication and exsanguination. The advantages of the drill hole model are that it is highly reproducible and does not require a metal fixation device, leading to fewer postsurgical complications compared with other fracture models with mechanical instability (6, 25).

Generation of mice with type 1 diabetes. Male 8-week-old C57BL/6 mice from Envigo/Harlan were randomly divided into 4 groups: groups 1 and 2 (12 mice each) received streptozotocin at 100 mg/kg intraperitoneally for 2 days, while groups 3 and 4 (controls, 9 mice per group) received vehicle injections. Two weeks after the start of injections, glucose was measured in tail vein blood, and mice with a glucose concentration of more than 290 mg/dL were considered diabetic. Mice underwent surgery for placement of the monocortical defect 2 weeks later, as described above. One day postoperatively, the mice in groups 2 and 4 received vehicle or cinaciguat at 10 μg/kg/d intraperitoneally for 9 days. This dose of cinaciguat does not reduce systolic blood pressure significantly (18). On day 10, the mice were euthanized.

POB and BMSC cultures. POBs were explant cultures derived from fragments of femur and tibial shafts of 8-week-old male and female mice. Cells were isolated as described (55) and were cultured in DMEM with 10% FBS unless otherwise indicated; cells were used at passages 1–3, and each batch was characterized by alkaline phosphatase staining and mineralization capacity (14). To induce differentiation, cells were plated at high density and after confluence were switched to medium with 0.3 mM sodium ascorbate and 10 mM β-glycerophosphate.

BMSCs were collected by flushing bone marrow from femoral and tibial bones. After lysis of red blood cells, the remaining cells were plated at 4×10^5 cells/cm² in RPMI 1640 with 10% FBS/10% horse serum (18). After 7 days, adherent cells were switched to α-MEM supplemented with 10% FBS/10% horse serum, 0.3 mM sodium ascorbate, and 10 mM β-glycerolphosphate. Alkaline phosphatase staining was performed 14 days later.

qRT-PCR. After removing growth plates and bone marrow, bone shafts were snap-frozen in liquid N_2 and pulverized. RNA was purified from bone shafts and POBs, and qRT-PCR was performed with 300 ng of total RNA as described (17). All primers were tested with serial cDNA dilutions (Supplemental Table 3 and ref. 21).

Relative changes in mRNA expression were analyzed with 18S rRNA serving as an internal reference; the mean ΔCt obtained for control mice was used to calculate the fold change in mRNA expression in *Prkg1* OB-KO mice using the $2^{-\Delta\Delta Ct}$ method.

Western blotting, immunofluorescence, and immunohistochemical staining. Western blots were generated using horseradish peroxidase–conjugated secondary antibodies detected by enhanced chemoluminescence (26). POBs plated on glass coverslips were fixed in 4% paraformaldehyde, permeabilized with 1% Triton-X-100, and incubated with cleaved caspase-3–specific antibody (1:100 dilution), followed by a secondary FITC-conjugated antibody. For BrdU incorporation, cells were incubated with 200 μM BrdU for 16 hours; then cells were fixed, permeabilized, and incubated with DNase I before staining with anti-BrdU antibody (1:100 dilution) and secondary Texas Red–conjugated antibody (15). Nuclei were counterstained with Hoechst 33342, and images were analyzed with a Keyence BZ-X700 fluorescence microscope.

Tibiae were fixed overnight in 10% formalin, decalcified in 0.5 M EDTA (pH 7.5) for 5 days, and embedded in paraffin. Eight-micrometer sections were deparaffinized in xylene and rehydrated in graded ethanol and water. For antigen retrieval, slides were placed in 10 mM sodium citrate buffer (pH 6.0) at 80°C–85°C and allowed to cool to room temperature for 30 minutes. Endogenous peroxidase activity was quenched in 3% H_2O_2 for 10 minutes. After blocking with 5% normal goat serum, slides were incubated overnight at 4°C with anti-CD31 (1:100) or anti–phospho-Smad 1/5/8 antibody (1:100), followed by a horseradish peroxidase–conjugated secondary antibody (1 hour, room temperature). After development with 3,3-diaminobenzidine substrate (Vector Laboratories), slides were counterstained with hematoxylin.

μCT. Ethanol-fixed tibiae were analyzed using a Skyscan 1076 scanner at 9-μm voxel size and applying an electrical potential of 50 kVp and a current of 200 mA, with a 0.5-mm aluminum filter (17). Mineral density was determined by calibration of images against 2-mm–diameter hydroxyapatite rods (0.25 and 0.75 g/cm³). To measure regenerating bone, the VOI in the drill hole region was defined as a cylinder with a diameter of 0.65 mm (74 pixels) and a height of 0.3 mm (33 slices), extending from the outer surface of the tibia through the cortical bone (Supplemental Figure 3, A and B). Bone defects containing cortical bone fragments greater than 100 μm in the long axis were excluded from analysis. Three-dimensional images from the VOI were constructed using CTvol software. A global threshold (70–255) was chosen to identify trabecular bone in the defect area. Uninjured cortical bone was analyzed by automatic contouring 3.6 to 4.5 mm distal to the proximal growth plate, using a global threshold (100–255) to select cortical bone, and eroding 1 pixel to eliminate partial volume effects. Uninjured trabecular bone was analyzed by automatic contouring of the proximal tibial metaphysis (0.36 to 2.1 mm distal to the growth plate), using an adaptive threshold to select trabecular bone (17).

Histomorphometry. Tibiae were fixed, decalcified, and paraffin-embedded as described above, and Masson's trichrome–stained sections were used to count osteoblasts and osteoclasts on trabecular surfaces of uninjured bone, between 0.25 and 1.25 mm distal to the growth plate (17). For histological analysis of regenerating bone, paraffin-embedded tibiae with monocortical defects were sectioned sagittally and stained with Masson's trichrome. An area of 200 μm × 500 μm between the 2 cortical bone ends of the defect was analyzed (a 0.1-mm² "region of interest" marked by the black rectangle in Figure 2C). Only sections showing a fully intact region of interest were analyzed. Collagen content (percentage of the area of interest stained by aniline blue) was measured using Nanozoomer Digital Pathology NDP.view2 software.

For dynamic bone formation analyses, double calcein labeling was performed by intraperitoneal injection of calcein (25 mg/kg) at 7 and 2 days before euthanasia. Femurs were fixed in 10% neutral buffered formalin for 24 hours at room temperature and processed in 5% aqueous potassium hydroxide for 96 hours at room temperature, to allow sectioning of paraffin-embedded, nondecalcified bone samples (56). The percentage of single- and double-labeled BSs, and the double calcein interlabel width, were measured at trabecular and endocortical surfaces, to calculate MS (MS = [double-labeled BS + (0.5 × single-labeled BS)]/BS), MAR (MAR = interlabel width/labeling period), and BFR (BFR = MS × MAR) (23). Slides were scanned with a Hamamatsu Nanozoomer 2.0 HT Slide Scanning System, and image analysis was performed using the Nanozoomer Digital Pathology NDP.view2 software.

Statistics. Based on published data for the drill hole bone regeneration model (6), we calculated that it would take *n* = 7 mice to detect an absolute change of 10% in BV/TV (SD 6.5%) with 80% power, when measuring mineralized bone in the hole region by μCT (α error 0.05). For comparison of 2 groups, *P* values refer to unpaired, 2-tailed *t* test or to a 1-sample *t* test, as appropriate. For multiple comparisons, *P* values refer to either 1-way ANOVA followed by Bonferroni's multiple-comparisons test or 2-way ANOVA with Holm-Šidák multiple-comparisons test (e.g., to determine how POB genotype affected response to drug

treatment or serum starvation). $P < 0.05$ was considered statistically significant. When the assumption of equal variances was not met, a nonparametric test was also done (Mann-Whitney U test). Data analysis was performed using GraphPad Prism 7 software.

Study approval. All mouse experiments were approved by the Institutional Animal Care and Use Committee of the University of California, San Diego.

Author contributions

NS, JJG, AP, and RBP designed the study. NS, JJG, HK, and SPC conducted the study. NS, JJG, HK, SPC, and JJL collected data. NS, JJG, HK, and RBP analyzed data. NS, JJG, HK, RLS, AP, and RBP interpreted data. NS and RBP drafted the manuscript. NS, JJG, HK, and RBP take responsibility for the integrity of the data analysis. NS and JJG contributed similarly to this work, but JJG joined the project after NS had initiated the work.

Acknowledgments

Address correspondence to: Renate B. Pilz, University of California, San Diego, 9500 Gilman Drive, La Jolla, California 92093-0652, USA. Phone: 858.534.8805; Email: rpilz@health.ucsd.edu.

1. Hadjiargyrou M, O'Keefe RJ. The convergence of fracture repair and stem cells: interplay of genes, aging, environmental factors and disease. *J Bone Miner Res*. 2014;29(11):2307–2322.
2. Jiao H, Xiao E, Graves DT. Diabetes and its effect on bone and fracture healing. *Curr Osteoporos Rep*. 2015;13(5):327–335.
3. Fazzalari NL. Bone fracture and bone fracture repair. *Osteoporos Int*. 2011;22(6):2003–2006.
4. Sathyendra V, Darowish M. Basic science of bone healing. *Hand Clin*. 2013;29(4):473–481.
5. Tsuji K, et al. BMP2 activity, although dispensable for bone formation, is required for the initiation of fracture healing. *Nat Genet*. 2006;38(12):1424–1429.
6. Hu K, Olsen BR. Osteoblast-derived VEGF regulates osteoblast differentiation and bone formation during bone repair. *J Clin Invest*. 2016;126(2):509–526.
7. Kalyanaraman H, Schall N, Pilz RB. Nitric oxide and cyclic GMP functions in bone. *Nitric Oxide*. 2018;76:62–70.
8. Diwan AD, Wang MX, Jang D, Zhu W, Murrell GA. Nitric oxide modulates fracture healing. *J Bone Miner Res*. 2000;15(2):342–351.
9. Meesters DM, et al. Deficiency of inducible and endothelial nitric oxide synthase results in diminished bone formation and delayed union and nonunion development. *Bone*. 2016;83:111–118.
10. Armour KE, et al. Defective bone formation and anabolic response to exogenous estrogen in mice with targeted disruption of endothelial nitric oxide synthase. *Endocrinology*. 2001;142(2):760–766.
11. Watanuki M, et al. Role of inducible nitric oxide synthase in skeletal adaptation to acute increases in mechanical loading. *J Bone Miner Res*. 2002;17(6):1015–1025.
12. Marathe N, Rangaswami H, Zhuang S, Boss GR, Pilz RB. Pro-survival effects of 17β-estradiol on osteocytes are mediated by nitric oxide/cGMP via differential actions of cGMP-dependent protein kinases I and II. *J Biol Chem*. 2012;287(2):978–988.
13. Rangaswami H, et al. Protein kinase G and focal adhesion kinase converge on Src/Akt/β-catenin signaling module in osteoblast mechanotransduction. *J Biol Chem*. 2012;287(25):21509–21519.
14. Kalyanaraman H, et al. Nongenomic thyroid hormone signaling occurs through a plasma membrane-localized receptor. *Sci Signal*. 2014;7(326):ra48.
15. Rangaswami H, et al. Cyclic GMP and protein kinase G control a Src-containing mechanosome in osteoblasts. *Sci Signal*. 2010;3(153):ra91.
16. Lundberg JO, Gladwin MT, Weitzberg E. Strategies to increase nitric oxide signalling in cardiovascular disease. *Nat Rev Drug Discov*. 2015;14(9):623–641.
17. Kalyanaraman H, et al. A novel, direct NO donor regulates osteoblast and osteoclast functions and increases bone mass in ovariectomized mice. *J Bone Miner Res*. 2017;32(1):46–59.
18. Kalyanaraman H, et al. Protein kinase G activation reverses oxidative stress and restores osteoblast function and bone formation in male mice with type 1 diabetes. *Diabetes*. 2018;67(4):607–623.
19. Pfeifer A, Aszódi A, Seidler U, Ruth P, Hofmann F, Fässler R. Intestinal secretory defects and dwarfism in mice lacking cGMP-dependent protein kinase II. *Science*. 1996;274(5295):2082–2086.
20. Pfeifer A, et al. Defective smooth muscle regulation in cGMP kinase I-deficient mice. *EMBO J*. 1998;17(11):3045–3051.
21. Ramdani G, et al. cGMP-dependent protein kinase-2 regulates bone mass and prevents diabetic bone loss. *J Endocrinol*. 2018;238(3):203–219.
22. Dacquin R, Starbuck M, Schinke T, Karsenty G. Mouse alpha1(I)-collagen promoter is the best known promoter to drive efficient Cre recombinase expression in osteoblast. *Dev Dyn*. 2002;224(2):245–251.
23. Dempster DW, et al. Standardized nomenclature, symbols, and units for bone histomorphometry: a 2012 update of the report of the ASBMR Histomorphometry Nomenclature Committee. *J Bone Miner Res*. 2013;28(1):2–17.

24. Kim JB, et al. Bone regeneration is regulated by wnt signaling. *J Bone Miner Res*. 2007;22(12):1913–1923.

25. He YX, et al. Impaired bone healing pattern in mice with ovariectomy-induced osteoporosis: A drill hole defect model. *Bone*. 2011;48(6):1388–1400.

26. Rangaswami H, et al. Type II cGMP-dependent protein kinase mediates osteoblast mechanotransduction. *J Biol Chem*. 2009;284(22):14796–14808.

27. Hu K, Olsen BR. Vascular endothelial growth factor control mechanisms in skeletal growth and repair. *Dev Dyn*. 2017;246(4):227–234.

28. Dulak J, et al. Nitric oxide induces the synthesis of vascular endothelial growth factor by rat vascular smooth muscle cells. *Arterioscler Thromb Vasc Biol*. 2000;20(3):659–666.

29. Wu M, Chen G, Li YP. TGF-β and BMP signaling in osteoblast, skeletal development, and bone formation, homeostasis and disease. *Bone Res*. 2016;4:16009.

30. Deckers MM, et al. Bone morphogenetic proteins stimulate angiogenesis through osteoblast-derived vascular endothelial growth factor A. *Endocrinology*. 2002;143(4):1545–1553.

31. Schwappacher R, et al. Novel crosstalk to BMP signalling: cGMP-dependent kinase I modulates BMP receptor and Smad activity. *EMBO J*. 2009;28(11):1537–1550.

32. Farkas K, Jermendy G, Herold M, Ruzicska E, Sasvári M, Somogyi A. Impairment of the NO/cGMP pathway in the fasting and postprandial state in type 1 diabetes mellitus. *Exp Clin Endocrinol Diabetes*. 2004;112(5):258–263.

33. Riddle RC, et al. Lrp5 and Lrp6 exert overlapping functions in osteoblasts during postnatal bone acquisition. *PLoS One*. 2013;8(5):e63323.

34. Wang T, Zhang X, Bikle DD. Osteogenic differentiation of periosteal cells during fracture healing. *J Cell Physiol*. 2017;232(5):913–921.

35. Street J, et al. Vascular endothelial growth factor stimulates bone repair by promoting angiogenesis and bone turnover. *Proc Natl Acad Sci U S A*. 2002;99(15):9656–9661.

36. Jacobsen KA, et al. Bone formation during distraction osteogenesis is dependent on both VEGFR1 and VEGFR2 signaling. *J Bone Miner Res*. 2008;23(5):596–609.

37. Ziche M, Morbidelli L. Nitric oxide and angiogenesis. *J Neurooncol*. 2000;50(1-2):139–148.

38. Józkowicz A, et al. Involvement of nitric oxide in angiogenic activities of vascular endothelial growth factor isoforms. *Growth Factors*. 2004;22(1):19–28.

39. Kawasaki K, Smith RS, Hsieh CM, Sun J, Chao J, Liao JK. Activation of the phosphatidylinositol 3-kinase/protein kinase Akt pathway mediates nitric oxide-induced endothelial cell migration and angiogenesis. *Mol Cell Biol*. 2003;23(16):5726–5737.

40. Bettaga N, Jäger R, Dünnes S, Groneberg D, Friebe A. Cell-specific impact of nitric oxide-dependent guanylyl cyclase on arteriogenesis and angiogenesis in mice. *Angiogenesis*. 2015;18(3):245–254.

41. Aicher A, et al. cGMP-dependent protein kinase I is crucial for angiogenesis and postnatal vasculogenesis. *PLoS One*. 2009;4(3):e4879.

42. Jin E, et al. Differential roles for ETS, CREB, and EGR binding sites in mediating VEGF receptor 1 expression in vivo. *Blood*. 2009;114(27):5557–5566.

43. Jeon SH, et al. The PKA/CREB pathway is closely involved in VEGF expression in mouse macrophages. *Mol Cells*. 2007;23(1):23–29.

44. Gudi T, Casteel DE, Vinson C, Boss GR, Pilz RB. NO activation of fos promoter elements requires nuclear translocation of G-kinase I and CREB phosphorylation but is independent of MAP kinase activation. *Oncogene*. 2000;19(54):6324–6333.

45. Onishi T, et al. Distinct and overlapping patterns of localization of bone morphogenetic protein (BMP) family members and a BMP type II receptor during fracture healing in rats. *Bone*. 1998;22(6):605–612.

46. Khan MP, et al. BMP signaling is required for adult skeletal homeostasis and mediates bone anabolic action of parathyroid hormone. *Bone*. 2016;92:132–144.

47. Dai J, Li L, Jiang C, Wang C, Chen H, Chai Y. Bone morphogenetic protein for the healing of tibial fracture: a meta-analysis of randomized controlled trials. *PLoS One*. 2015;10(10):e0141670.

48. Peng H, et al. VEGF improves, whereas sFlt1 inhibits, BMP2-induced bone formation and bone healing through modulation of angiogenesis. *J Bone Miner Res*. 2005;20(11):2017–2027.

49. Sun N, et al. Modified VEGF-A mRNA induces sustained multifaceted microvascular response and accelerates diabetic wound healing. *Sci Rep*. 2018;8(1):17509.

50. Kondo E, et al. Increased bone turnover and possible accelerated fracture healing in a murine model with an increased circulating C-type natriuretic peptide. *Endocrinology*. 2015;156(7):2518–2529.

51. Shuhaibar LC, et al. Dephosphorylation of the NPR2 guanylyl cyclase contributes to inhibition of bone growth by fibroblast growth factor. *Elife*. 2017;6:e31343.

52. Stasch JP, et al. Targeting the heme-oxidized nitric oxide receptor for selective vasodilatation of diseased blood vessels. *J Clin Invest*. 2006;116(9):2552–2561.

53. Lim JC, et al. TNFα contributes to diabetes impaired angiogenesis in fracture healing. *Bone*. 2017;99:26–38.

54. Haas B, et al. Protein kinase G controls brown fat cell differentiation and mitochondrial biogenesis. *Sci Signal*. 2009;2(99):ra78.

55. Bakker A, Klein-Nulend J. Osteoblast isolation from murine calvariae and long bones. *Methods Mol Med*. 2003;80:19–28.

56. Porter A, Irwin R, Miller J, Horan DJ, Robling AG, McCabe LR. Quick and inexpensive paraffin-embedding method for dynamic bone formation analyses. *Sci Rep*. 2017;7:42505.